Molecular basis of mannose recognition by pradimicins and their application to microbial cell surface imaging

Yu Nakagawa,[1,2,*] Takashi Doi,[3] K. Takegoshi,[3] Takahiro Sugahara,[4] Dai Akase,[4] Misako Aida,[4] Kazue Tsuzuki,[1] Yasunori Watanabe,[1] Tomohiko Tomura,[1] Makoto Ojika,[1] Yasuhiro Igarashi,[5] Daisuke Hashizume,[6] and Yukishige Ito[2]

[1]Department of Applied Biosciences, Graduate School of Bioagricultural Sciences, Nagoya University, Furo-cho, Chikusa-ku, Nagoya 464-8601, Japan

[2]Synthetic Cellular Chemistry Laboratory, RIKEN, 2-1 Hirosawa, Wako, Saitama 351-0198, Japan

[3]Department of Chemistry, Graduate School of Science, Kyoto University, Kitashirakawa Oiwake-cho, Sakyo-ku, Kyoto 606-8502, Japan

[4]Center for Quantum Life Sciences, and Department of Chemistry, Graduate School of Science, Hiroshima University, 1-3-1 Kagamiyama, Higashi-Hiroshima, Hiroshima 739-8526, Japan

[5]Biotechnology Research Center, Toyama Prefectural University, 5180 Kurokawa, Imizu, Toyama 939-0398, Japan

[6]RIKEN Center for Emergent Matter Science (CEMS), 2-1 Hirosawa, Wako, Saitama 351-0198, Japan

*Correspondence: yu@agr.nagoya-u.ac.jp

SUMARRY

Naturally-occurring pradimicins (PRMs) show specific recognition of D-mannose (D-Man) in aqueous media, which has never been achieved by artificial small molecules. Although the Ca^{2+}-mediated dimerization of PRMs is essential for their D-Man binding, the dimeric structure has yet to be elucidated, leaving the question open as to how PRMs recognize D-Man. Thus, we herein report the structural elucidation of the dimer by a combination of X-ray crystallography and solid-state NMR spectroscopy. Coupled with our previous knowledge regarding the D-Man binding geometry of PRMs, elucidation of the dimer allowed reliable estimation of the mode of D-Man binding. Based on the binding model, we further developed an azide-functionalized PRM derivative (PRM-Azide) with D-Man-binding specificity. Notably, PRM-Azide stained *Candida rugosa* cells having mannans on their cell surface through conjugation with the tetramethylrhodamine fluorophore. The present study provides the first practical demonstration that PRMs can serve as lectin mimics for use in glycobiological studies.

KEYWORDS

Analog design, Carbohydrates, Glycan detection, Lectin, Molecular recognition, Natural products, Structural elucidation

INTRODUCTION

Overwhelming evidence exists to demonstrate that carbohydrates are involved in a variety of biological events such as fertilization, embryogenesis, cell proliferation, immune response, pathogen infection, and tumour progression (Ohtsubo and Marth, 2006; Paulson et al., 2006; Pinho and Reis, 2015; Varki, 2017). It is therefore recognized that a comprehensive study of carbohydrates is essential to achieve a detailed understanding of such physiological and pathological processes. Lectins have been employed as a tool to dissect the structure and function of carbohydrates (Alley et al., 2013; Dan et al., 2016; Hendrickson and Zherdev, 2018). However, their applications have often been hampered by cross-reactivity problems originating from their low carbohydrate specificity. In addition, lectins have several disadvantages, as the large-scale production of proteins is often limited by cost and time concerns, and their long-term storage and chemical modification tend to be challenging. From a therapeutic viewpoint, they have unfavourable properties, such as a susceptibility to enzymatic degradation, immunogenicity, cytotoxicity, inflammation, and hemagglutination. These issues have collectively impeded the widespread use of lectins for biotechnological and therapeutic purposes, thereby leading to a growing demand for the development of carbohydrate-binding small molecules that are chemically stable and can be easily tuned for structural optimization.

The predominant issue in terms of carbohydrate recognition by small molecules is the competition between carbohydrates and water molecules (Davis, 2009; Yang et al. 2011). More specifically, the polyol structure of carbohydrates is easily reproduced by clusters of water molecules, rendering them difficult to capture in aqueous solvents. Another fundamental problem is selectivity among carbohydrates. For example, the complete discrimination of D-glucose (D-Glc) from D-mannose (D-Man), D-galactose (D-Gal), and D-glucosamine is prohibitively burdensome, as they differ only in one stereochemistry or in one functional group. As a consequence, the recognition of one specific carbohydrate by small molecules in water is particularly challenging.

To address the above issues, several strategies have been pursued in the area of supramolecular chemistry (Davis, 2009; Miron and Petitjean, 2015; Yang et al., 2011). The use of boronic acids, which form reversible covalent bonds with 1,2- or 1,3-diols,

represents one strategy to bind carbohydrates in water (Jin et al., 2010; Zhai et al., 2015). Tripod- and cage-shaped molecules can act as lectin mimics, which accommodate carbohydrates through non- covalent interactions (Davis, 2009; Gentili et al., 2016; Mazik, 2012; Park et al., 2015). Although promising, these molecules tend to suffer from a lack of potency in water, a low selectivity among carbohydrates, or both. One prominent exception is Davis's cage-shaped molecules, which selectively recognize carbohydrates exhibiting an all-equatorial array of polar functionalities in water (Ferrand et al., 2007; Ferrand et al., 2009; Ke et al., 2012; Sookcharoenpinyo et al., 2012). However, despite advances in our understanding of factors contributing carbohydrate recognition (Asensio, et al., 2013; Francesconi et al., 2018; Roldós et al., 2011; Tromans et al., 2019; Yang et al., 2011), there remains a general lack of synthetic small molecules that bind one specific carbohydrate under physiological conditions.

On the other hand, nature produces a unique class of carbohydrate-binding small molecules. Pradimicins (PRMs, Figure 1a) and benanomicins are actinomycete-derived antibiotics that bind D-Man in the presence of Ca^{2+} ions (Fukagawa et al., 1993; Oki et al., 1988; Takeuchi et al., 1988). These natural products completely discriminate D-Man from the majority of common monosaccharides, including D-Glc, D-Gal, *N*-acetyl-D-glucosamine (D-GlcNAc), *N*-acetyl-D-galactosamine (D-GalNAc), and L-fucose (L-Fuc), under physiologically relevant conditions (Ueki et al., 1993a). Additionally, and quite significantly, PRMs exhibit antifungal, antiviral, and antiparasitic activities through binding to D-Man-containing glycans of pathogenic species (Alen et al., 2011; Balzarini, 2007; Castillo-Acosta et al., 2016; François and Balzarini, 2012; Igarashi and Oki, 2004). Such glycan-targeted antipathogenic behavior has yet to be observed in existing chemotherapeutics, thereby highlighting their potential as promising drugs for the treatment of infectious diseases.

Despite their exceptional D-Man-binding properties and medicinally important biological activities, the structural modification of PRMs for research and therapeutic uses has been impeded by limited knowledge of their D-Man recognition mechanism. Indeed, three key interconnected issues render the analysis of such interactions challenging. Firstly, PRMs bear a disaccharide moiety, whose ^{1}H and ^{13}C NMR signals overlap with those of

D-Man. Secondly, PRMs form multiple complexes and associated species in solution (Figure 1b). More specifically, two PRM molecules are initially bridged by Ca^{2+} to afford the binary [PRM_2/Ca^{2+}] complex, which accommodates four molecules of D-Man over two separate steps (Fujikawa et al., 1998; Ueki et al., 1993b). These [PRM_2/Ca^{2+}], [PRM_2/Ca^{2+}/D-Man_2], and [PRM_2/Ca^{2+}/D-Man_4] complexes randomly assemble with one another to give a complicated mixture of associated species. Thirdly, the ternary complexes have a high propensity to aggregate, and so are unsuitable for crystallization. These issues have thereby complicated the structural analyses of the ternary complexes by X-ray crystallographic and solution NMR approaches.

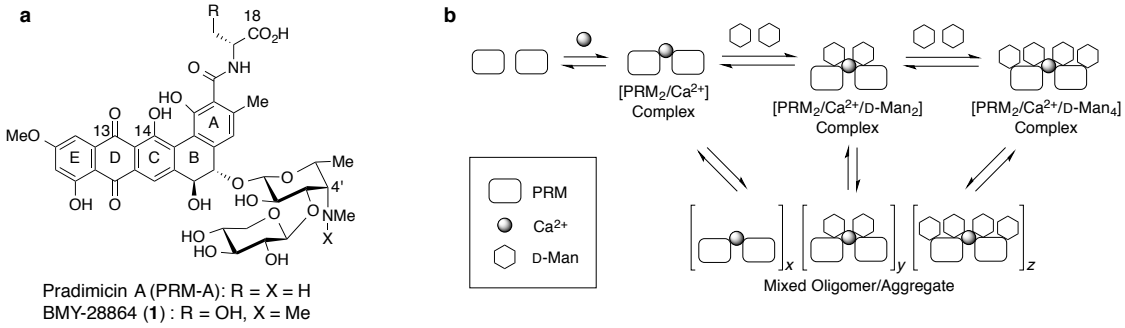

Figure 1. Pradimicins and their complex-forming process with Ca^{2+} and D-Man. (a) Chemical structures of pradimicins used in this study. (b) PRMs form the [PRM_2/Ca^{2+}] complex, which binds two molecules of D-Man with high affinity. The resulting [PRM_2/Ca^{2+}/D-Man_2] complex accommodates another two molecules of D-Man with low affinity to give the ultimate [PRM_2/Ca^{2+}/D-Man_4] complex. These three complexes randomly assemble with one another to afford the mixed oligomers or aggregates.

To address these issues, we previously developed a novel analytical approach based on solid-state NMR spectroscopy (Nakagawa et al., 2011a;. Nakagawa et al., 2011b; Nakagawa et al., 2013) Although significant efforts have been made to avoid the aggregation of PRMs, our approach actually makes use of the inherent aggregating properties of PRM-A (Figure 1a), a flagship member of PRMs, to prepare a solid sample mainly composed of the [PRM_2/Ca^{2+}/D-Man_2] complex. The use of this solid aggregate eliminates the issue of the complicated equilibrium in solution, while allowing one-to-one interaction analysis of PRM-A and D-Man. Our approach also involves selective ^{13}C labeling of the aglycon moiety of PRM-A to discriminate the ^{13}C signals of PRM-A from

those of D-Man, thereby greatly facilitating spectral interpretation. Using this approach, our dipolar-assisted rotational resonance (DARR) technique (Takegoshi et al., 2001; Takegoshi et al., 2003) successfully revealed that the C2–C4 region of D-Man is in close contact with PRM-A, with the C2 and C3 positions oriented toward the ABC rings and the D-alanine moiety, respectively, in the complex. However, a lack of data regarding the geometry of Ca^{2+} coordination prevented us from estimating the mode of D-Man binding. Here, we report structural determination of the [PRM_2/Ca^{2+}] complex through a combination of X-ray crystallography and solid-state NMR spectroscopy, which allows a reliable estimation of the mechanism of D-Man recognition by PRM-A. We also disclose that an azide-functionalized derivative of PRM-A completely discriminates D-Man from other common monosaccharides in aqueous media, and fluorescently stains the cell wall mannans of *Candida rugosa*.

RESUTS AND DISCUSSION

Structural Elucidation of the [PRM_2/Ca^{2+}] Complex

Among the range of natural and semi-synthetic PRM derivatives reported to date, BMY-28864 (**1**, Figure 1a), which contains D-serine instead of the D-alanine moiety of PRM-A, was selected for crystal preparation of the [PRM_2/Ca^{2+}] complex because of its excellent solubility in water (Oki et al., 1990). We found that **1** exhibited limited aggregation at a concentration of 1 mM in a 3-morpholinopropane-1-sulfonic acid (MOPS) buffer (pH 7.0) containing 10 mM $CaCl_2$, thereby resulting in the formation of X-ray quality crystals in this solution system at 4 °C. The crystal structure was then analyzed at a resolution of 0.77 Å (Figure 2a, also see STAR Methods). As expected from our recent solid-state NMR study based on the use of $^{111}Cd^{2+}$ as a surrogate probe for Ca^{2+} for evaluation of the ^{13}C–^{111}Cd distances (Doi et al., 2017), the 13-carbonyl and 14-hydroxyl groups of **1** were found to coordinate with Ca^{2+} to bridge the anthraquinone moieties of two molecules of **1**. In this dimeric structure, the A–D rings stack antiparallel to one another, while the E rings face the amide moieties (Figure 2b). This face-to-face geometry suggests that, in addition to Ca^{2+} coordination, aromatic π–π stacking contributes to formation of the

[PRM_2/Ca^{2+}] complex.

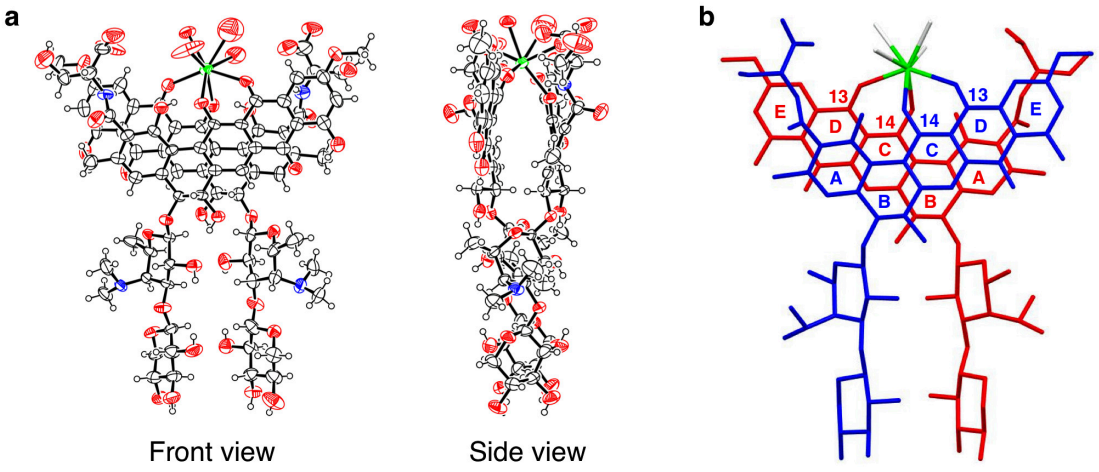

Figure 2. Molecular structure of the [$\mathbf{1}_2/Ca^{2+}$] complex. (a) ORTEP drawing of the [$\mathbf{1}_2/Ca^{2+}$] complex. Thermal ellipsoids are drawn at the 50% probability level. (b) Two molecules of **1** in the [$\mathbf{1}_2/Ca^{2+}$] complex are separately shown in red and blue. Hydrogen atoms are omitted for clarity.

However, it must also be confirmed whether the crystal structure truly reflects the dimeric form of PRM-A in the aggregate of the [PRM-A_2/Ca^{2+}/D-Man_2] complex. Thus, we examined the dimeric geometry of PRM-A in the aggregate by two-dimensional (2D) dipolar-assisted rotational resonance (DARR) experiments. DARR (Takegoshi et al., 2001; Takegoshi et al., 2003), which is also known as radio-frequency-assisted diffusion (Morcombe et al., 2004), is a solid-state NMR technique that is employed to observe weak ^{13}C–^{13}C couplings in the presence of strong ^{13}C–^{13}C couplings derived from directly bound carbon atoms. In a 2D-DARR spectrum, coupled pairs of ^{13}C nuclei that are located within ~6 Å can be simultaneously detected as cross-peaks. Given that the intermolecular proximity (i.e., <6 Å) between the 11-*O*-methyl group and the D-serine moiety of **1** is characteristic of the face-to-face geometry of the crystal structure (Figure 3a), we performed DARR analysis to evaluate the interatomic distances between the 11-*O*-methyl group and the D-alanine moiety of PRM-A in the aggregate of the [PRM_2/Ca^{2+}/D-Man_2] complex.

We previously demonstrated that the addition of DL-[$^{13}C_3$]alanine to the culture broth of PRM-A-producing *Actinomadura* sp. TP-A0019 significantly increased the

^{13}C-population of the D-alanine moiety of the isolated PRM-A (Nakagawa et al., 2013). In

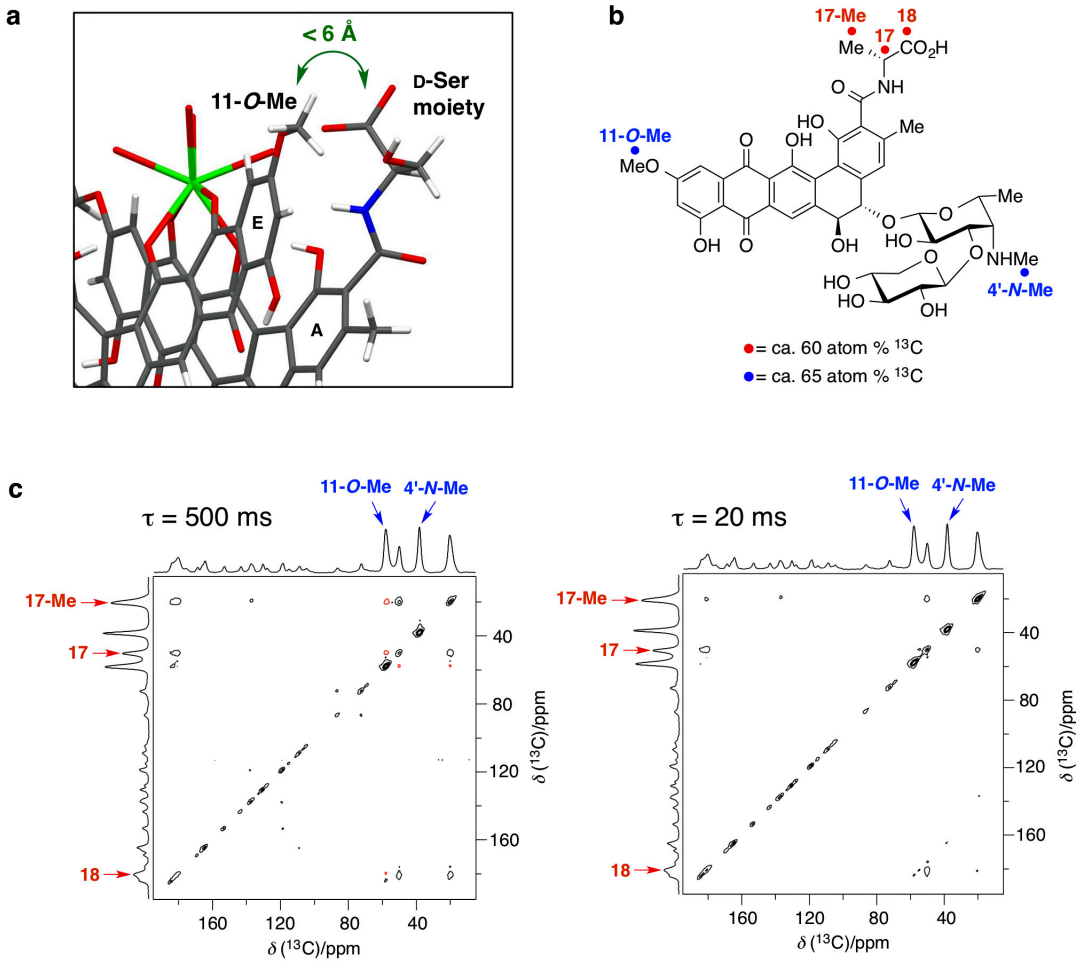

Figure 3. DARR analysis of the [PRM-A$_2$/Ca^{2+}/D-Man-OMe$_2$] complex. (a) Enlarged view of the dimeric structure. Carbon, oxygen, nitrogen, hydrogen, and calcium atoms are shown in gray, red, blue, white, and green, respectively. The 11-*O*-methyl group of one molecule of **1** is in the proximity of the D-serine moiety of the other. (b) ^{13}C-enriched PRM-A used in DARR analysis. Red (ca. 60 atom % ^{13}C) and blue (ca. 65 atom % ^{13}C) circles indicate ^{13}C-enriched positions. The ^{13}C population of the aromatic moiety was also slightly increased (ca. 15 atom % ^{13}C). The ^{13}C population was calculated from solution ^{1}H-NMR data on the basis of integration values of proton signals split with ^{1}H–^{13}C couplings. (c) 2D-DARR spectra of the [PRM-A$_2$/Ca^{2+}/D-Man-OMe$_2$] complex at the mixing times of 500 ms (left) and 20 ms (right). Blue and red arrows represent ^{13}C signals of ^{13}C-enriched positions.

addition, the 11-*O*- and 4′-*N*-methyl groups were effectively ^{13}C-enriched by the feeding of L-[5-^{13}CH$_3$]methionine (Nakagawa et al., 2011b). Based on these earlier studies, we conducted the simultaneous feeding of DL-[^{13}C$_3$]alanine and L-[5-^{13}CH$_3$]methionine to

afford PRM-A bearing a ^{13}C-enriched D-alanine moiety (~60 atom% ^{13}C) and two enriched methyl groups (~65 atom% ^{13}C). Using this ^{13}C-labeled PRM-A (Figure 3b, for its ^{13}C-NMR spectrum, see Figure S1), we prepared the solid aggregate of the [PRM$_2$/Ca^{2+}/D-Man$_2$] complex using methyl α-D-mannopyranoside (D-Man-OMe) according to our standardized procedure (Nakagawa et al., 2011b, see STAR Methods). The obtained 2D-DARR spectra of the complex are shown in Figure 3c. As shown, in the spectrum obtained at a mixing time of 500 ms, symmetric cross-peaks were observed between ^{13}C signals for the D-alanine moiety (δ = 20.4 ppm for 17-Me, δ = 50.1 ppm for C17, and δ = 180.6 ppm for C18) and the 11-*O*-methyl group (δ = 58.1 ppm). The absence of these cross-peaks at a mixing time of 20 ms indicates that they originate from ^{13}C–^{13}C coupling reintroduced by DARR during mixing time. In contrast, the mixing time-dependent cross peaks were generally not detected in the case of the 4′-*N*-methyl signal (δ = 38.2 ppm), thereby eliminating the possibility that the cross-peaks between ^{13}C signals of the D-alanine moiety and the 11-*O*-methyl group are derived from non-specific contacts between PRM-A molecules in the solid aggregate. These combined results indicate that the D-alanine moiety is located within 6 Å of the 11-*O*-methyl group in the aggregate of the [PRM$_2$/Ca^{2+}/D-Man$_2$] complex. Considering the intramolecular distance between these moieties (>10 Å), this proximity suggests that two PRM-A molecules would be arranged in the face-to-face geometry as also indicated by the obtained crystal structure.

Estimation of the [PRM$_2$/Ca^{2+}/D-Man$_2$] complex

Following confirmation that the crystal structure almost reflects the dimeric form in the aggregate of the [PRM$_2$/Ca^{2+}/D-Man$_2$] complex, we performed molecular modeling to estimate the mode of D-Man binding of PRM-A. Our previous DARR studies (Nakagawa et al., 2013) revealed that in the [PRM$_2$/Ca^{2+}/D-Man$_2$] complex, the C2 and C3 positions of D-Man are oriented toward the ABC rings and the D-alanine moiety of PRM-A, respectively (Figure 4a). In addition, solid-state ^{113}Cd-NMR analysis previously suggested that Ca^{2+} adopted a dual role, namely as a core to bridge two PRM-A molecules, and as a direct participant in D-Man binding (Nakagawa et al., 2011a). Given the proximity of the C2 position of D-Man to the anthraquinone moiety of PRM-A, it is quite likely that the latter

role of Ca^{2+} involves its coordination to the 2-hydroxyl group of D-Man. Based on these results, an initial structure was proposed for the [PRM-A_2/Ca^{2+}/D-Man-OMe_2] complex by replacing two of the four Ca^{2+}-coordinated water molecules with the 2-hydroxyl group of D-Man-OMe, followed by optimization through density functional theory (DFT) calculations at the ωB97X-D/6-31G(d) level of theory.

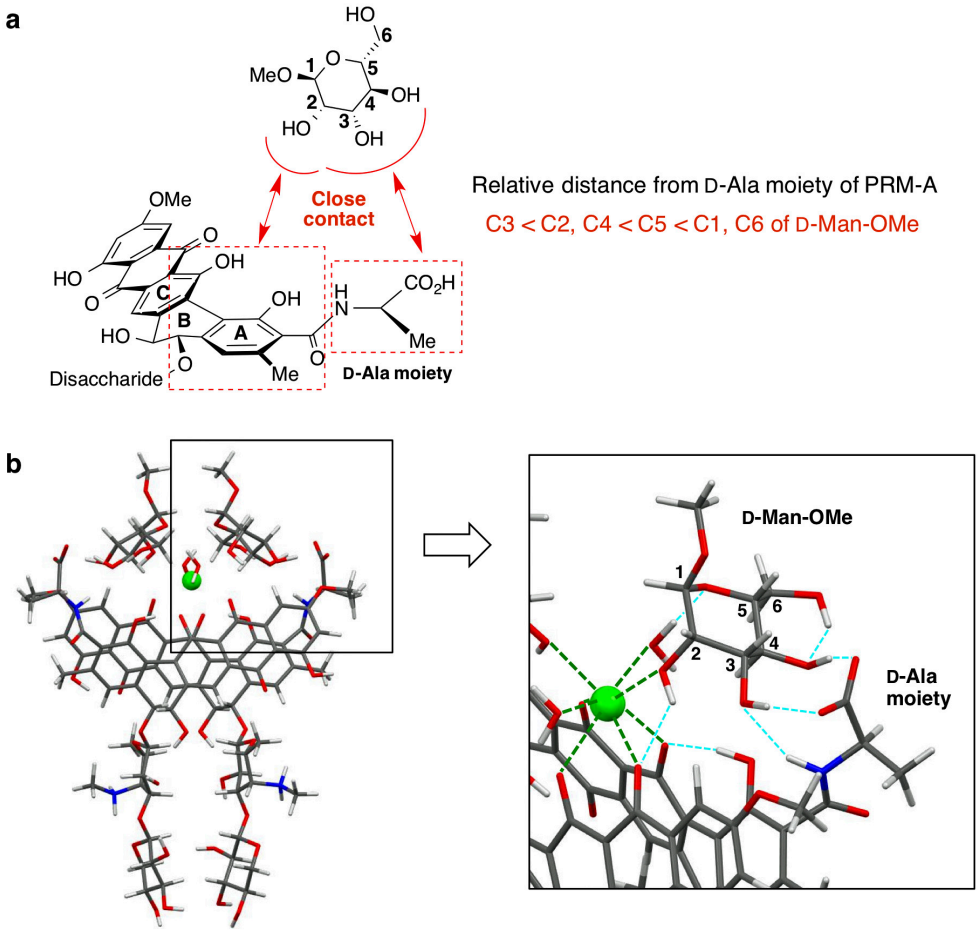

Figure 4. Solid-state NMR-based structure of the [PRM-A_2/Ca^{2+}/D-Man-OMe_2] complex. (a) Relative geometry of PRM-A and D-Man-OMe in the [PRM-A_2/Ca^{2+}/D-Man_2] complex obtained by previous DARR analysis. (b) Energy-minimized structure of the [PRM-A_2/Ca^{2+}/D-Man-OMe_2] complex obtained by DFT calculations. Carbon, oxygen, nitrogen, hydrogen, and calcium atoms are shown in gray, red, blue, white, and green, respectively. (c) Possible interaction of PRM-A with D-Man-OMe in the [PRM-A_2/Ca^{2+}/D-Man-OMe_2] complex. Hydrogen bonding and Ca^{2+} coordination are indicated as blue and green dotted lines, respectively.

Thus, the obtained energy-minimized structure is shown in Figure 4b, where it is

apparent that two molecules of D-Man-OMe bind to the [PRM-A_2/Ca^{2+}] complex in an almost symmetric fashion. In accordance with previous DARR studies (Nakagawa et al., 2013), the C2–C4 region of D-Man-OMe was found to be located close to the D-alanine moiety of PRM-A, with the shortest interatomic distance of approximately 3.3 Å being calculated between the C3 atom of D-Man-OMe and the C18 atom of PRM-A (see Figure S2 for details). In this binding geometry, the 2-, 3-, and 4-hydroxyl groups of D-Man-OMe form hydrogen bonds with PRM-A, and an additional hydrogen bond is found between the oxygen atom in the pyranose ring of D-Man-OMe and the Ca^{2+}-coordinated water molecule. However, the 6-hydroxyl group of D-Man-OMe does not interact with either Ca^{2+} or PRM-A. This binding mode is therefore in perfect agreement with the fact that PRM-A recognizes the 2-, 3-, and 4-hydroxyl groups but not the 6-hydroxyl group of D-Man (Nakagawa et al., 2013), and accounts for the excellent D-Man specificity of PRM-A.

Development of PRM-Azide (2)

Following elucidation of the molecular origin of D-Man recognition by PRM-A, we then wished to identify a site within the PRM-A molecule that could be readily modified to prepare derivatives for glycobiological studies. One conceivable site was the 4′-NHMe group (Figure 1a), which is located far from the D-Man binding region, and thus would be suitable for modification without affecting the D-Man binding ability. However, a recent study into PRM-functionalized gold nanoparticles indicated that the introduction of a linker to this group was arduous and material-consuming (Enomoto et al., 2015). The 18-carboxyl group was therefore considered more promising from the viewpoint of ease of chemical modification, but efforts to modify this group were previously abandoned because of the perception that it may be involved in Ca^{2+} coordination (Ueki et al., 1993c). However, as we herein confirmed that the anthraquinone moiety rather than the carboxyl group is responsible for Ca^{2+}-binding, we decided to explore the possibility that an azide-functionalized polyethylene glycol (PEG) could be introduced into the carboxyl group. The amide linkage was selected for this purpose as our preliminary modeling using PRM-Amide (Figure 5a) suggested that the amide hydrogen could act as a hydrogen bond donor for the C4 hydroxyl group of D-Man, thereby leading to retention of the D-Man

binding specificity. In addition, an earlier study reported that several amide derivatives of PRM-A exhibit antifungal activity, which is related to the D-Man binding ability (Nishio et al., 1993), and facile formation of the amide linkage through an ester/amide exchange reaction using PRM-A methyl ester would produce the desired functionality without the requirement for the protection of other functional groups within the molecule.

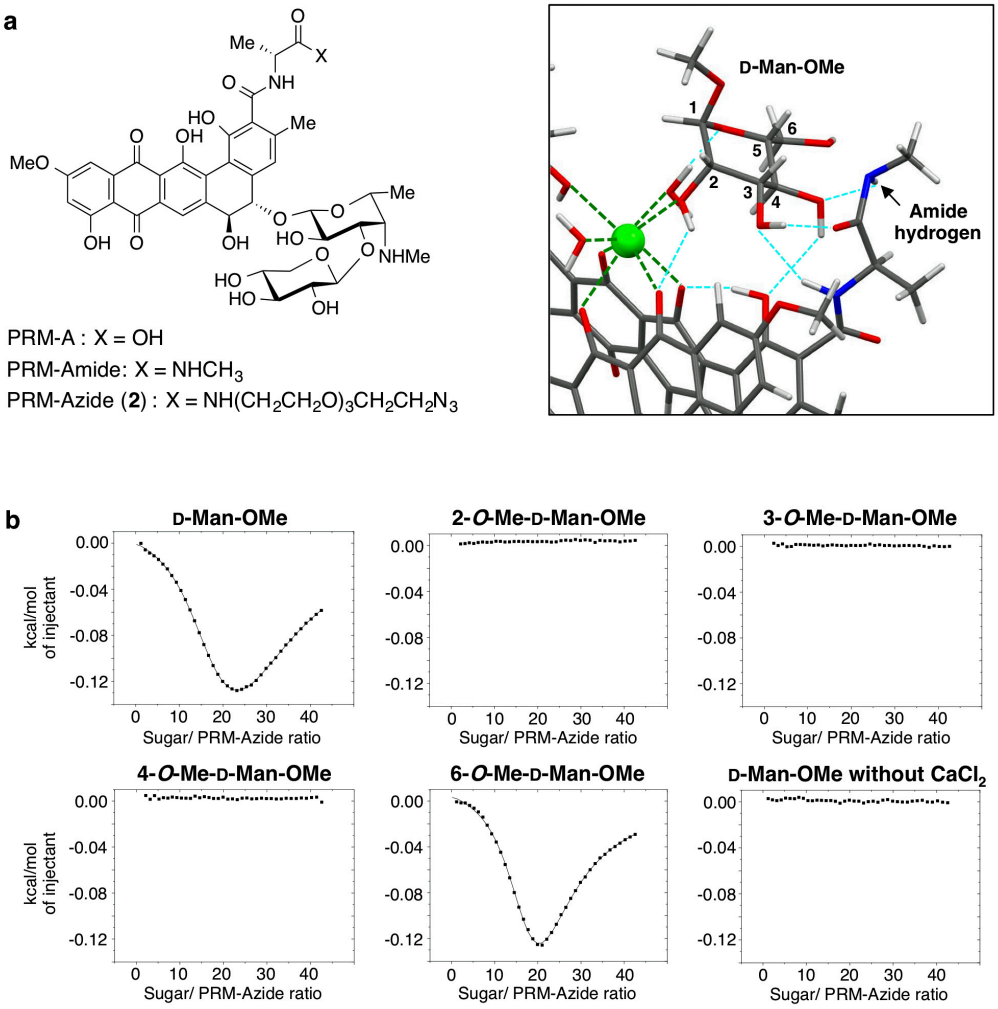

Figure 5. Design and D-Man binding of PRM-Azide (2). (a) Chemical structures of PRM-Amide and PRM-Azide (**2**) (left), and possible interaction of PRM-Amide with D-Man-OMe (right). Carbon, oxygen, nitrogen, hydrogen, and calcium atoms are shown in gray, red, blue, white, and green, respectively. Hydrogen bonding and Ca^{2+} coordination are indicated as blue and green dotted lines, respectively. (b) ITC profiles for **2** titrated with D-Man-OMe and its *O*-methyl derivatives. The ITC experiments were performed using 1 mM **2** and 200 mM sugar in 50 mM MOPS buffer (pH 7.0) with or without 10 mM $CaCl_2$ at 30 °C. The solid lines in

the titration with D-Man-OMe and 6-*O*-methyl-D-Man-OMe represent the least-squares fit of the data to a two-site binding model.

These considerations led us to prepare PRM-Azide (**2**, Figure 5a), in which 11-azido-3,6,9-trioxaundecan-1-amine is attached to the carboxyl group of PRM-A *via* the amide linkage. As expected, **2** was successfully synthesized from PRM-A in only two steps (for preparation and characterization of **2**, see STAR Methods and Figure S3). Following its preparation, we initially evaluated the ability of **2** to bind D-Man-OMe based on isothermal titration calorimetry (ITC) studies. Thus, the titration of **2** with D-Man-OMe in the presence of $CaCl_2$ gave an isotherm curve characteristic of the D-Man binding of PRM-A (Figure 5b). The least-squares fit of the data to a two-site binding model provided K_1 and K_2 values of 1,950 and 123 M^{-1} (Table 1, see STAR Methods for thermodynamic parameters and Figure S4 for raw ITC data), respectively, suggesting that modification had no deleterious effect on D-Man binding (K_1 = 10,400 M^{-1}, K_2 = 263 M^{-1} for PRM-A, Nakagawa et al., 2011b).

Table 1. K_a values for monosaccharide binding of PRM-Azide (2)

Monosaccharide	K_1 (M^{-1})[a]	K_2 (M^{-1})[a]
D-Man-OMe	1,950 ± 244	123 ± 12
2-*O*-Me-D-Man-OMe	~0[b]	
3-*O*-Me-D-Man-OMe	~0[b]	
4-*O*-Me-D-Man-OMe	~0[b]	
6-*O*-Me-D-Man-OMe	2,190 ± 384	147 ± 15
D-Mannose	1,680 ± 178	64 ± 5.2
L-Mannose	~0[b]	
N-Acetyl-D-mannosamine	~0[b]	
D-Glucose	~0[b]	
D-Galactose	~0[b]	
N-Acetyl-D-glucosamine	~0[b]	
N-Acetyl-D-galactosamine	~0[b]	
L-Fucose	~0[b]	
N-Acetylneuraminic acid methyl ester[c]	~0[b]	
D-Allose	~0[b]	
L-Sorbose	~0[b]	
D-Talose	~0[b]	
L-Rhamnose	~0[b]	
L-Gulose	~0[b]	

[a]Determined by ITC experiments. [b]Too small to be determined. [c]*N*-Acetylneuraminic acid could not be used due to severe pH change

during titration.

Additional ITC experiments using *O*-methyl derivatives of D-Man-OMe (Chervenak and Toone, 1996) revealed that **2** was responsive to the 6-*O*-methyl derivative but not to its 2-*O*-, 3-*O*-, and 4-*O*-methyl counterparts (Table 1, for raw ITC data, see Figure S4). Furthermore, only negligible binding was observed in the titration with D-Man-OMe in the absence of $CaCl_2$ (see Figure S4). These results collectively indicate that the Ca^{2+} complex of **2** interacts with the 2-, 3-, and 4-hydroxyl groups of D-Man-OMe, thereby supporting our design strategy. Moreover, ITC experiments confirmed that **2** completely discriminates D-Man from other common monosaccharides (Table 1, for raw ITC data, see Figure S4).

Fluorescent Staining of *Candida rugosa* Cells Using PRM-Azide (2)

Following the above confirmation that the D-Man binding specificity was retained following modification, we then explored the application of **2** in glycobiological studies. We initially connected **2** to the tetramethylrhodamine (TAMRA) fluorophore *via* a copper-catalyzed azide–alkyne cycloaddition (CuAAC) reaction (Rostovtsev et al., 2002; Hong et al., 2009) to develop a fluorescent dye for staining the D-Man-containing glycans (Figure 6a). Unfortunately, the resulting conjugate PRM-TAMRA (**3**) exhibited no detectable D-Man binding under the ITC conditions. A plausible rationale is that the TAMRA moiety disturbs the π-π stacking between two molecules of **2**, and as a consequence, inhibits formation of the [PRM_2/Ca^{2+}] complex. We therefore examined whether the TAMRA fluorophore can be connected to **2** following complex formation with Ca^{2+} and D-Man. High performance liquid chromatographic (HPLC) analysis confirmed that the CuAAC reaction of **2** with the TAMRA-alkyne cleanly provided **3** in $CaCl_2$-containing MOPS buffer (see Figure S6 for details). The reaction was found to decelerate but clearly proceed even following the pre-incubation of **2** with an excess of D-Man-OMe in the same solvent system, suggesting that complex formation does not completely disturb conjugation with the TAMRA fluorophore.

Given the encouraging results obtained for the conjugation reaction in the presence of Ca^{2+} and D-Man-OMe, we subsequently focused on the fluorescent staining of

glycans on living cells. Earlier studies demonstrated that **1** binds to mannans present on fungal cell surfaces (Ueki et al., 1993b), and so we wished to determine whether *Candida*

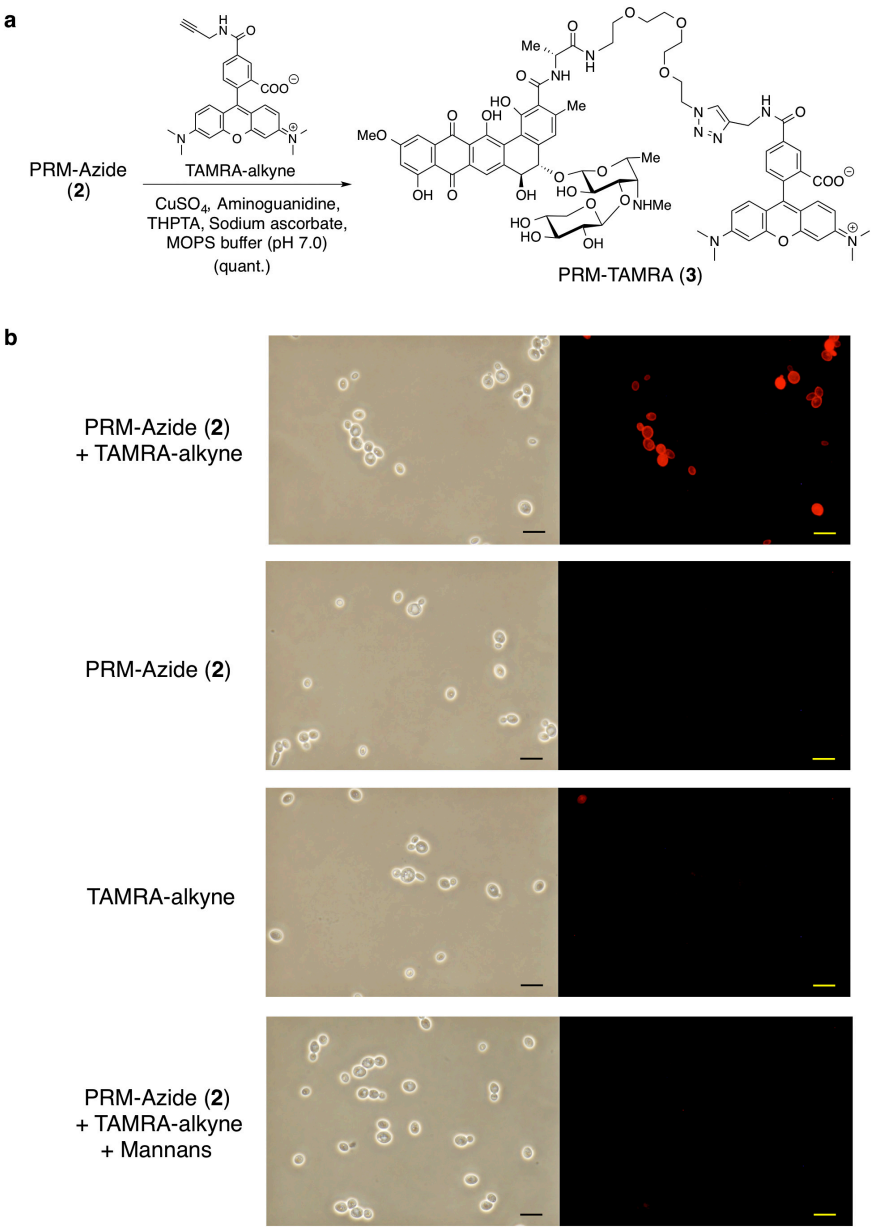

Figure 6. Conjugation of PRM-Azide (2) with the TAMRA fluorophore and fluorescent staining of fungal mannans. (a) CuAAC reaction of **2** and TAMRA-alkyne to afford PRM-TAMRA (**3**). THPTA = tris(3-hydroxypropyltriazoylmethyl)amine. (b) Phase-contrast (left) and fluorescent (right) images of *Candida rugosa* after treatment of **2** and/or TAMRA-alkyne under CuAAC reaction conditions. Yeast cells were pre-incubated with **2** and/or TAMRA-alkyne in the absence or presence of exogenous mannans derived from *Saccharomyces cerevisiae* before CuAAC reaction. Scale bars, 10 μm.

rugosa cells could be stained with **2**. As shown in Figure 6b, clear fluorescence was observed on the fungal cells following treatment with **2** and a subsequent CuAAC reaction with the TAMRA-alkyne. The absence of either **2** or TAMRA-alkyne resulted in a marked reduction or complete absence of fluorescence, and the fluorescent staining was suppressed by exogenous mannans derived from *Saccharomyces cerevisiae*, suggesting that the observed fluorescence arises from a complex of **3** with the cell wall mannans of *C. rugosa*. In contrast, only faint fluorescence was observed when *Escherichia coli*, which bears cell wall glycans consisting of D-GlcNAc and *N*-acetylmuramic acid, was treated according to the same procedure (see Figure S7). These combined observations indicate that **2** appears to be suitable for the selective staining of D-Man-containing glycans. Upon considering the advantages of PRMs over protein lectins in regard to chemical stability and cellular uptake, **2** has also a potential to be used for positron emission tomography (PET) imaging of intracellular glycans by connecting with radiolabelled tags though CuAAC reaction. Further application of this probe in glycobiological context is currently underway, and will be reported in due course.

SIGNIFICANCE

Despite the growing biological and pathological significance of D-Man-containing glycans, there is a general lack of small molecules that specifically capture D-Man under physiological conditions. Although PRMs have been considered to hold great promise as drug leads for carbohydrate-related diseases and as research tools in glycobiology, limited knowledge regarding their D-Man recognition mechanism has hampered their structural optimization and modification. Here, we successfully determined the structure of the [PRM_2/Ca^{2+}] complex, which allowed a reliable estimation of the structure of the [PRM_2/Ca^{2+}/D-Man_2] complex showing the molecular basis of D-Man recognition by PRM-A. Based on the obtained binding model, we further demonstrated that an azide-functionalized PEG moiety can be introduced into the carboxyl group of PRM-A, with the only cost being a modest decrease in the D-Man binding affinity. Notably, the

resulting derivative, PRM-Azide (**2**), showed D-Man-specific recognition in aqueous media, and successfully stained *C. rugosa* cells having mannans on their cell surface through conjugation with the TAMRA fluorophore. Upon considering that PRM-A is now commercially available and the azide group provides a handle for chemical modification *via* Click chemistry, we predict that **2** will serve as a versatile tool in glycobiological studies visualizing cell surface glycans.

ACNOWLEDGMENTS

This work was partly supported by JSPS KAKENHI Grant (Number JP15H04496) and SUNBOR GRANT from the Suntory Foundation of Life Sciences. *Candida rugosa* AJ 14513 (NBRC 0750) and *Escherichia coli* AJ 3837 (NBRC 14237) were provided from Ajinomoto Co., Inc. (Kanagawa, Japan). The DFT calculations were partly carried out at the Research Center for Computational Science, Okazaki, Japan. We thank Mr. Kazushi Koga for NMR spectroscopic assistance.

AUTHOR CONTRIBUTIONS

Y.N. and Y.It. conceived the project, and Y.N. designed the experiments. Y.N. and Y.Ig. prepared the samples for the X-ray crystallographic and DARR experiments. D.H. performed X-ray crystallographic analysis, T.D. and K.Ta performed DARR experiments, and T.S., D.A. and M.A. performed DFT calculations. Y.N., K.Ts. and Y.W. synthesized PRM-Azide and *O*-methyl derivatives of D-Man-OMe. Y.N. conducted ITC experiments. K.Ts., T.T. and M.O. performed fluorescent staining. Y.N. wrote the manuscript and all authors were engaged in its editing.

DECLARATION OF INTERESTS

The authors declare no competing financial interests.

REFERENCES

Alen, M.M.F., Burghgraeve, T.D., Kaptein, S.J.F., Balzarini, J., Neyts, J., and Schols, D. (2011). Broad antiviral activity of carbohydrate-binding agents against the four serotypes of dengue virus in monocyte-derived dendritic cells. PLoS ONE *6,* e21658.

Alley, W.R.Jr., Mann, B.F., and Novotny, M.V. (2013). High-sensitivity analytical approaches for the structural characterization of glycoproteins. Chem. Rev. *113,* 2668–2732.

Asensio, J.L., Ardá, A., Cañada, F.J., and Jiménez-Barbero, J. (2013). Carbohydrate–aromatic interactions. Acc. Chem. Res. *46,* 946–954.

Balzarini, J. (2007). Targeting the glycans of glycoproteins: A novel paradigm for antiviral therapy. Nat. Rev. Microbiol. *5,* 583–597.

Burla, M.C., Caliandro, R. Camalli, M., Carrozzini, B., Cascarano, G.L., De Caro, L., Giacovazzo, C., Polidori, G., and Spagna, R. (2005). SIR2004: an improved tool for crystal structure determination and refinement. J. Appl. Cryst. 38, 381–388.

Castillo-Acosta, V.M., Ruiz-Pérez, L.M., Etxebarria, J., Reichardt, N.C., Navarro, M., Igarashi, Y., Liekens, S., Balzarini, J., and González-Pacanowska, D. (2016). Carbohydrate-binding non-peptidic pradimicins for the treatment of acute sleeping sickness in murine models. PLoS Pathog. *12,* e1005851.

Chai, J.-D., and Head-Gordon, M. (2008) Long-range corrected hybrid density functionals with damped atom-atom dispersion corrections. Phys. Chem. Chem. Phys. *10*, 6615–6620.

Chervenak, M.C., and Toone, E.J. (1996). Analysis of the binding specificities of oligomannoside-binding proteins using methylated monosaccharides. Bioorg. Med. Chem. *4,* 1963–1977.

Dan, X., Liu, W., and Ng, T.B. (2016). Development and applications of lectins as biological tools in biomedical research. Med. Res. Rev. *36,* 221–247.

Davis, A.P. (2009). Synthetic lectins. Org. Biomol. Chem. *7,* 3629–3638.

Doi, T. Nakagawa, Y., and Takegoshi, K. (2017). Solid-state nuclear magnetic resonance analysis reveals a possible calcium binding site of pradimicin A. Biochemistry *56,* 468–472.

Enomoto, M., Igarashi, Y., Sasaki, M., and Shimizu, H. (2015). A mannose-recognizable chemosensor using gold nanoparticles functionalized with pradimicin, a nonpeptidic mannose-binding natural product. Tetrahedron *71,* 2603–2609.

Ferrand, Y., Crump, M.P., and Davis, A.P. (2007). A synthetic lectin analog for biomimetic disaccharide recognition. Science *318,* 619–622.

Ferrand, Y., Klein, E., Barwell, N.P., Crump, M.P., Jiménez-Barbero, J., Vicent, C., Boons, G.-J., Ingale, S., Davis A.P. (2009). A synthetic lectin for O-linked beta-*N*-acetylglucosamine. Angew. Chem. Int. Ed. *48,* 1775–1779.

François, K.O., and Balzarini, J. (2012). Potential of carbohydrate-binding agents as therapeutics against enveloped viruses. Med. Res. Rev. *32,* 349–387.

Francesconi, O., Martinucci, M., Badii, L., Nativi, C., and Roelens, S. (2018) A biomimetic synthetic receptor selectively recognizing fucose in water. Chem. Eur. J. *24*, 6828–6836.

Frisch, M.J., Trucks, G.W., Schlegel, H.B., Scuseria, G.E., Robb, M.A., Cheeseman, J.R., Scalmani, G., Barone, V., Mennucci, B., Petersson, G.A. et al., (2010). Gaussian 09, Revision C.01. Gaussian, Inc., Wallingford CT.

Fujikawa, K., Tsukamoto, Y., Oki, T., and Lee, Y.C. (1998). Spectroscopic studies on the interaction of pradimicin BMY-28864 with mannose derivatives. Glycobiology *8,* 407–414.

Fukagawa, Y., Ueki, T., Numata, K., and Oki, T. (1993). Pradimicins and benanomicins, sugar-recognizing antibiotics: Their novel mode of antifungal action and conceptual

significance. Actinomycetol. *7,* 1–22.

Gentili, M., Nativi, C., Francesconi, O., and Roelens, S. (2016). Synthetic receptors for molecular recognition of carbohydrates. Carbohydr. Chem. *41,* 149–186.

Hendrickson, O.D., and Zherdev. A.V. (2018). Analytical application of lectins. Crit. Rev. Anal. Chem. *48,* 279–292.

Hong, V., Presolski, S.I., Ma, C., and Finn, M.G. (2009). Analysis and optimization of copper-catalyzed azide–alkyne cycloaddition for bioconjugation. Angew. Chem. Int. Ed. *48,* 9879–9883.

Igarashi, Y., and Oki, T. (2004). Mannose-binding quinone glycoside, MBQ: Potential utility and action mechanism. Adv. Appl. Microbiol. *54,* 147–166.

Jin, S., Cheng, Y., Reid, S., Li, M., and Wang, B. (2010). Carbohydrate recognition by boronolectins, small molecules, and lectins. Med. Res. Rev. *30,* 171–257.

Ke, C., Destecroix, H., Crump, M.P., and Davis, A.P. (2012). A simple and accessible synthetic lectin for glucose recognition and sensing. Nat. Chem. *4,* 718–723.

Mazik, M. (2012). Recent developments in the molecular recognition of carbohydrates by artificial receptors. RSC Advances *2,* 2630–2642.

Miron, C.E., and Petitjean, A. (2015). Sugar recognition: Designing artificial receptors for applications in biological diagnostics and imaging. ChemBioChem *16,* 365–379.

Nakagawa, Y., Masuda, Y., Yamada, K., Doi, T., Takegoshi, K., Igarashi, Y., and Ito, Y. (2011a). Solid-state NMR spectroscopic analysis of the Ca^{2+}-dependent mannose binding of pradimicin A. Angew. Chem. Int. Ed. *50,* 6084–6088.

Nakagawa, Y., Doi, T., Masuda, Y., Takegoshi, K., Igarashi, Y., and Ito, Y. (2011b). Mapping of the primary mannose binding site of pradimicin A. J. Am. Chem. Soc. *133,* 17485–17493.

Nakagawa, Y., Doi, T., Taketani, T., Takegoshi, K., Igarashi, Y., and Ito, Y. (2013). Mannose-binding geometry of pradimicin A. Chem. Eur. J. *19,* 10516–10525.

Nishio, M., Ohkuma, H., Kakushima, M., Ohta, S., Iimura, S., Hirano, M., Konishi M., and Oki, T. (1993). Synthesis and antifungal activities of pradimicin A derivatives modification of the alanine moiety. J. Antibiot. *46*, 494–499.

Ohtsubo, K., and Marth, J.D. (2006). Glycosylation in cellular mechanisms of health and

disease. Cell *126*, 855–867.

Oki, T., Konishi, M., Tomatsu, K., Tomita, K., Saitoh, K., Tsunakawa, M., Nishio, M., Miyaki, T., and Kawaguchi, H. (1988). Pradimicin, a novel class of potent antifungal antibiotics. J. Antibiot. *41,* 1701–1704.

Oki, T., Kakushima, M., Nishio, M., Kamei, H., Hirano, M., Sawada, Y., and Konishi, M. (1990). Water-soluble pradimicin derivatives, synthesis and antifungal evaluation of *N*,*N*-dimethyl pradimicins. J. Antibiot. *43,* 1230–123.

Morcombe, C.R., Gaponenko, V., Byrd, R.A., and Zilm, K.W. (2004). Diluting abundant spins by isotope edited radio frequency field assisted diffusion. J. Am. Chem. Soc. *126,* 7196–7197.

Park, S.H., Choi, Y.P., Park, J., Share, A., Francesconi, O., Nativi, C., Namkung, W., Sessler, J.L., Roelens, S., and Shin, I. (2015) Synthetic aminopyrrolic receptors have apoptosis inducing activity. Chem. Sci. 6, 7284–7292.

Paulson, J.C., Blixt, O., and Collins, B.E. (2006). Sweet spots in functional glycomics. Nat. Chem. Biol. *2*, 238–248.

Pinho, S.S., and Reis, C.A. (2015). Glycosylation in cancer: Mechanisms and clinical implications. Nat. Rev. Cancer *15*, 540–555.

Roldós, V., Cañada, F.J., and Jiménez-Barbero, J. (2011). Carbohydrate-protein interactions: A 3D view by NMR. ChemBioChem *12,* 990–1005.

Rostovtsev, V.V., Green, L.G., Fokin, V.V., and Sharpless K.B. (2002). A stepwise Huisgen cycloaddition process: Cupper(I)-catalyzed regioselective “ligation” of azides and terminal alkynes. Angew. Chem. Int. Ed. *41,* 2596–2599.

Sheldrick, G.M. (2015). Crystal structure refinement with SHELXL. Acta Crystallogr. Sect. C *71,* 3–8.

Sookcharoenpinyo, B., Klein, E., Ferrand, Y., Walker, D.B., Brotherhood, P.R., Ke, C., Crump, M.P., and Davis A.P. (2012). High-affinity disaccharide binding by tricyclic synthetic lectins. Angew. Chem. Int. Ed. *51,* 4586–4590.

Takegoshi, K., Nakamura, S., and Terao, T. (2001). ^{13}C–^{1}H dipolar-assisted rotational resonance in magic-angle spinning NMR. Chem. Phys. Lett. *344,* 631–637.

Takegoshi, K., Nakamura, S., and Terao, T. (2003). ^{13}C–^{1}H dipolar-driven ^{13}C–^{13}C

recoupling without ^{13}C rf irradiation in nuclear magnetic resonance of rotating solids. J. Chem. Phys. *118,* 2325–2341.

Takeuchi, T., Hara, T., Naganawa, H., Okada, M., Hamada, M., Umezawa, H., Gomi, S., Sezaki, M., and Kondo, S. (1988). New antifungal antibiotics, benanomicins A and B from an actinomycete. J. Antibiot. *41,* 807–811.

Tromans, R.A., Carter, T.S., Chabanne, L., Crump, M.P., Li, H., Matlock, J.V., Orchard, M.G., and Davis, A.P. (2019). A biomimetic receptor for glucose. Nat. Chem. *11*, 52–56.

Ueki, T., Oka, M., Fukagawa, Y., and Oki, T. (1993a). Studies on the mode of antifungal action of pradimicin antibiotics III. Spectrophotometric sequence analysis of the ternary complex formation of BMY-28864 with D-mannopyranoside and calcium. J. Antibiot. *46,* 465–477.

Ueki, T., Numata, K., Sawada, Y., Nakajima, T., Fukagawa, Y., and Oki, T. (1993b). Studies on the mode of antifungal action of pradimicin antibiotics I. Lectin-mimic binding of BMY-28864 to yeast mannan in the presence of calcium. J. Antibiot. *46,* 149–161.

Ueki, T., Numata, K., Sawada, Y., Nishio, M., Ohkura, H., Kamachi, H., Fukagawa Y., and Oki, T. (1993c). Studies on the mode of antifungal action of pradimicin antibiotics II. D-Mannopyranoside-binding site and calcium-binding site. J. Antibiot. *46,* 455–464.

Varki, A. (2017). Biological roles of glycans. Glycobiology *27*, 3–49.

Yang, X., Cheng, Y., and Wang, B. (2011). Synthetic lectin mimics artificial carbohydrate receptors. In Carbohydrate recognition: biological problems, methods, and applications, B. Wang, and G.-J. Boons, ed. (Wiley, Hoboken), pp 301–327.

Zhai, W., Sun, X., James, T.D., and Fossey, J.S. (2015). Boronic acid-based carbohydrate sensing. Chem. Asian J. *10,* 1836–1848.

STAR METHODS

CONTACT FOR REAGENT AND RESOURCE SHARING

Further information and requests for resources and reagents should be directed to and will be fulfilled by the Lead Contact, Yu Nakagawa (yu@agr.nagoya-u.ac.jp).

EXPERMENTAL MODEL AND SUBJECT DETAILS

Candida rugosa AJ 14513 (NBRC 0750) was grown in YM broth at 30 °C. *Escherichia coli* AJ 3837 (NBRC 14237) was grown in LB broth at 37 °C.

METHOD DETAILS

General Remarks

HPLC was carried out using an L-2130 HPLC system (Hitachi). Solution NMR spectra were measured on a JEOL ECX 400 (^{1}H at 400 MHz, ^{13}C at 100 MHz), a Bruker AVANCE 400 (^{1}H at 400 MHz, ^{13}C at 100 MHz), or a Bruker AVANCE 600 (^{1}H at 600 MHz, ^{13}C at 150 MHz) magnetic resonance spectrometer. ^{1}H chemical shifts are reported relative to the residual solvent peak (DMSO = 2.50 ppm). ^{13}C chemical shifts are reported relative to the residual deuterated solvent ^{13}C signals (DMSO = 39.52 ppm). Signal assignments were made *via* 2D spectroscopy (COSY, HSQC, and HMBC). Optical rotation data were obtained using a JASCO DIP-370 digital polarimeter. High-resolution mass spectra were obtained using an Applied Biosystems Mariner ESI-TOF spectrometer.

X-ray Crystal Structure Analysis of the [$\mathbf{1_2/Ca^{2+}}$] Complex

Block red crystals were grown at 4 °C from a 1 mM solution of 1 in 50 mM MOPS buffer (pH 7.0) containing 10 mM $CaCl_2$. A single crystal with the dimensions of 0.12 x 0.12 x 0.07 mm was mounted on a MicroMount^{TM} (MiTeGen, LLC) and set on a Rigaku AFC-8 diffractometer with a Saturn70 CCD detector. The diffraction data were collected using MoKα radiation, which was monochromated by a multi-layered confocal mirror. The unit cell dimensions were determined using 170135 reflections with $3.48 \leq 2\theta \leq 54.96°$. The diffraction data of 170024 within $3.48 \leq 2\theta \leq 54.96°$ were collected and merged to give 25060 unique reflections with the R_{int} of 0.0692. The structure was solved by a direct method and refined on F^2 by a least-squares method by the programs SIR2004 (Burla et al., 2005) and SHELXL-2018/3 (Sheldrick, 2015), respectively. The final R values against 16161 unique reflections ($2\theta_{max} = 54.96°$) with $I > 2\sigma(I)$ are 0.0784 and 0.2176 for the $R(F)$ and the $wR(F^2)$, respectively. The absolute structure of the crystal was determined by anomalous dispersion effects ($\chi = 0.030(14)$). Detailed crystal data and structure refinement are as follows.

Formula	$C_{82}H_{96}N_4O_{42}Ca \cdot 19H_2O$
Formula weight	2192.01
Temperature	90 K
Wavelength	0.71073 Å

Crystal system	Hexagonal
Space group	$P6_5$
Unit cell dimensions	a = 21.3773(2) Å, c = 45.3383(5) Å
Volume	17943.3(4) Å^3
Z	6
Density (calculated)	1.217 Mg m^{-3}
Absorption coefficient	0.161 mm^{-1}
Crystal size	0.12 x 0.12 x 0.07 mm
Theta range for data collection	1.74 to 27.48°
Index ranges	$-27 \le h \le 27$, $-27 \le k \le 27$, $-58 \le l \le 41$
Reflections collected	170024
Independent reflections	25060 [R_{int} = 0.0692]
Completeness to theta = 27.48°	100.0 %
Absorption correction	None
Refinement method	Full-matrix least-squares on F^2
Data / restraints / parameters	25060 / 260 / 1423
Goodness-of-fit on F^2	1.041
Final R indices [$I > 2\sigma(I)$]	$R(F)$ = 0.0784, $wR(F^2)$ = 0.2176
R indices (all data)	$R(F)$ = 0.1185, $wR(F^2)$ = 0.2425
Absolute structure parameter	0.030(14)
$\Delta\rho_{max}$ and $\Delta\rho_{min}$	0.985 and −0.412 e Å^{-3}

Preparation of ^{13}C-Enriched PRM-A

Actinomadura sp. TP-A0019 was grown at 30 °C for 10 days on ISP-4 medium containing 0.2% yeast extract. The seed culture was incubated for 7 days at 30 °C in V22 medium (20 mL) in a 50-mL Erlenmeyer flask, and an aliquot (2.0 mL) was used as inocula to start fermentation. Aqueous solutions of DL-[$^{13}C_3$]alanine (100 mg/mL) and L-[5-$^{13}CH_3$]methionine (50 mg/mL) were sterilized by filtration, and an aliquot (2.0 mL) of each solution was added to A3M medium (100 mL) in a 50-mL Erlenmeyer flask before incubation. During incubation, addition of the L-[5-$^{13}CH_3$]methionine solution (2.0 mL) was continued in intervals of 1 day. After incubation for 6 days at 30 °C with shaking at 180 rpm, CH_3CN (100 mL) was added to the culture broth, and the mixture was shaken at 180 rpm for 2 h. The mycelia were separated by centrifugation at 12,000 rpm for 20 min. The supernatant was concentrated *in vacuo*, and the residue was adsorbed on a column of Diaion HP-20. After washing with water, the resin was eluted with 70% acetone/water containing 0.1% TFA and the eluate was concentrated *in vacuo*. The residue was purified by column chromatography (gel: YMC gel ODS-A; solvent: 20% → 30% CH_3CN/water containing 0.1%

TFA) to give crude ^{13}C-enriched PRM-A. Further purification was carried out by normal-phase HPLC (column: TSK gel Amide-80, 10 μm, 21.5 mm ID × 300 mm; solvent: 50-min linear gradient 95% → 63.5% CH_3CN/water containing 0.1% TFA: flow rate; 6.0 mL/min: UV; 254 nm) followed by reverse-phase HPLC (column: YMC-Pack ODS-A, 5 μm, 20.0 mm ID × 250 mm; solvent: 40-min linear gradient 25% → 37% CH_3CN/water containing 0.1% TFA: flow rate; 8.0 mL/min: UV; 254 nm) to afford pure ^{13}C-enriched PRM-A (8.5 mg) as a TFA salt. The ^{13}C-NMR spectrum (Figure S1) confirmed that ^{13}C-population at 11-*O*-Me, C17, 17-Me, C18, and 4'-*N*-Me positions of PRM-A was selectively increased.

Preparation of the Solid Aggregate Composed of the [PRM-A_2/Ca^{2+}/D-Man-OMe_2] Complex Using ^{13}C-Enriched PRM-A

To a 10 mM solution of ^{13}C-enriched PRM-A in distilled water (1.7 mL) were added 50 mM $CaCl_2$ (3.4 mL, 10 equiv.) and 100 mM D-Man-OMe (4.25 mL, 25 equiv.) at room temperature. The pH of the solution was adjusted to 4.5 with 1 N NaOH, and the resulting mixture was incubated at 60 °C for 2 h and then at 4 °C for 1 h. After centrifugation at 9,840 g for 20 min at 4 °C, the supernatant was removed by decantation. The precipitate was washed two times with 50 mM $CaCl_2$, and then dried in vacuo to afford the solid aggregate composed of the [PRM-A_2/Ca^{2+}/D-Man-OMe_2] complex (14.7 mg) as a red powder.

Two-Dimensional Dipolar Assisted Rotational Resonance (2D-DARR) Experiment

2D-DARR experiments were carried out at 14 T (150 MHz for ^{13}C) with a JEOL ECA600 spectrometer and a custom-fabricated probe with a Chemagnetics 3.2 mm spinning system at a MAS frequency of 15 kHz and room temperature. Ramped-amplitude CP (Ramp-CP) and two-pulse phase-modulated (TPPM) decoupling were used. Pulse sequence parameters were: contact time of 1.25-1.75 ms, proton decoupling power of 70 kHz, t_1 increments of 33 μs, number of scans of 16 per increment, t_1 points of 256, mixing time of 20 ms or 500 ms, and pulse delay of 3 s. Chemical shifts were calibrated in ppm relative to TMS by taking the ^{13}C chemical shift for the methine ^{13}C of solid adamantane (29.5 ppm) as an external reference standard.

Molecular Modeling by DFT calculation

Initial structures of the [PRM-A_2/Ca^{2+}/D-Man-OMe_2] complex were built as follows. On the basis of binding geometry (Figure 4a) obtained by our previous solid-state NMR analysis (Nakagawa et al., 2013), two molecules of D-Man-OMe were docked to the crystal structure of the [PRM-A_2/Ca^{2+}] complex by replacing two Ca^{2+}-coordinated water molecules with the 2-hydroxyl group of D-Man-OMe, and with the C3 carbon atom of D-Man-OMe oriented toward D-alanine moiety of PRM-A. The resulting initial structures were used for the geometry optimization with a dispersion-corrected, long-range corrected hybrid density functional ωB97X-D (Chai et al., 2008) and the 6-31G(d) basis set. The most stable complex was adopted among the calculated geometries. The Gaussian 09 program package (Frisch et al., 2010) was used for all the DFT calculations. The calculations were carried out at the Center for Quantum Life Sciences (QuLiS) and at the Research Center for Computational Science, Okazaki National Research Institutes.

Synthesis and Characterization of PRM-Azide (2)

To a solution of PRM-A (TFA salt, 31.2 mg, 32.7 μmol) in MeOH (5.6 mL) was added 14% HCl/dioxane (56 μL). The reaction mixture was heated at reflux for 2 hr, and then directly loaded onto a Diaion HP-20 column. After washing with water, the resin was eluted with 80% acetone/water containing 0.1% TFA and the eluate was concentrated *in vacuo* to afford PRM-A methyl ester as a TFA salt (30.4 mg, 31.4 μmol, 96%). To a solution of PRM-A methyl ester (11.5 mg, 11.9 μmol) in MeOH (0.1 mL) was added 11-azido-3,6,9-trioxaundecan-1-amine (0.3 mL, 1.51 mmol). The reaction mixture was stirred at room temperature for 27 hr, and then directly loaded onto a Diaion HP-20 column. After washing with water, the resin was eluted with 80% acetone/water containing 0.1% TFA and the eluate was concentrated *in vacuo*. The residue was purified by reverse-phase HPLC (system: Hitachi L-2130, column: YMC-Pack ODS-A, 5 μm, 20.0 mm ID × 250 mm; solvent: 40 min linear gradient 25–60% CH_3CN/water containing 0.1% TFA; flow rate: 8.0 mL/min; UV: 254 nm; Rt: 26.1 min) to afford **2** (8.7 mg, 7.54 μmol, 63%) as a TFA salt.

*Characterization data for **2***

$[\alpha]_D$: +23.8 (*c* = 0.19 in MeOH, 30 °C)

HRMS (ESI) : *m/z* = 1041.3935 ([M + H^+]). Calcd. For $C_{48}H_{61}N_6O_{20}$, 1041.3968.

^{1}H-NMR (600 MHz, DMSO-d_6) and ^{13}C-NMR (150 MHz, DMSO-d_6) spectra are shown in Figure S3.

Signal assignments are shown below.

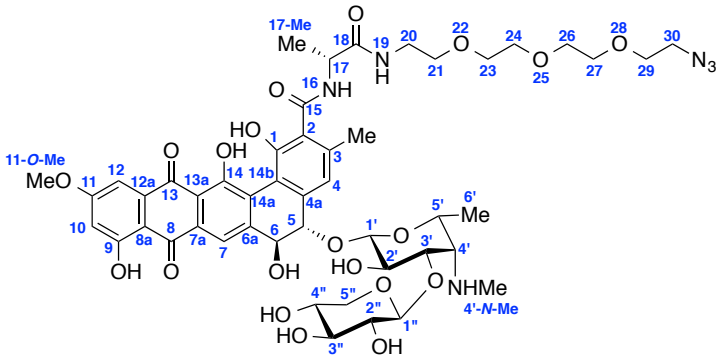

^{1}H-NMR and ^{13}C-NMR signal assignments for PRM-Azide (**2**).

Position	^{1}H-NMR (600 Hz)	^{13}C-NMR (125 Hz)
1		152.1
2		127.7
3		136.5
3-Me	2.29 (3H, s)	19.0
4	7.10 (1H, br.s)	118.1
4a		137.4
5	4.61 (1H, d, *J* = 8.6 Hz)	80.7
6	4.67 (1H, d, *J* = 8.6 Hz)	71.1
6a		146.9
7	7.99 (1H, br.s)	116.2
7a		131.3
8		185.3
8a		110.1
9		164.5
10	6.91 (1H, d, *J* = 1.6 Hz)	106.4
11		165.9
11-OMe	3.96 (3H, s)	56.2
12	7.30 (1H, d, *J* = 1.6 Hz)	107.3
12a		134.9
13		186.2
13a		116.2
14		158.4
14a		127.1
14b		114.8
15		167.0
16 (NH)	8.29 (1H, d, *J* = 7.6 Hz)	
17	4.47 (1H, m)	48.4
17-Me	1.32 (3H, d, *J* = 7.2 Hz)	17.5
18		172.1

1’	4.77 (1H, d, *J* = 7.6 Hz)	103.7
2’	3.54 (1H, m)	69.2
3’	3.98 (1H, m)	79.5
4’	3.44 (1H, m)	63.0
4’-NMe	2.69 (3H, s)	36.1
5’	3.92 (1H, br.q, *J* = 6.7 Hz)	67.3
6’	1.29 (3H, d, *J* = 6.7 Hz)	15.9
1’’	4.48 (1H, d, *J* = 7.3 Hz)	104.9
2’’	3.16 (1H, dd, *J* = 8.6, 7.3 Hz)	73.4
3’’	3.19 (1H, dd, *J* = 8.7, 8.5 Hz)	75.8
4’’	3.32 (1H, m)	69.0
5’’	3.14 (1H, dd, *J* = 11.3, 10.6 Hz), 3.77 (1H, dd, *J* = 11.3, 5.3 Hz)	65.7
19 (NH)	7.91 (1H, br.s)	
20	3.28 (2H, m)	38.6
21	3.29-3.61 (12H, m)	68.5
23		69.4, 69.5, 69.6 (3C)
24		
26		
27		
29		
30	3.36 (2H, m)	49.9

ITC Experiment

ITC measurements were carried out in 50 mM MOPS buffer (pH 7.0) containing 10 mM $CaCl_2$ at 30 °C using a Microcal iTC_{200} microcalorimeter (Microcal Inc., Northampton, MA). A typical titration consisted of injecting 1.0 μL of 200 mM (for D-Man-OMe and its *O*-methyl derivatives) or 400 mM (for D-Man and monosaccharides used in Table 1) sugar solution (total 40 injections) into 1 mM **2** with an interval of 2 min between injections at the stirrer speed of 1,000 rpm. The heat of dilution was determined under identical conditions by injecting the sugar solution into the ITC cell containing only the buffer. For every experiment, the heat of dilution was subtracted from the sample titration data before processing. The titration data were analyzed using the software provided by the manufacturer (Origin for ITC). The binding isotherm was fitted using two-site binding model to calculate the binding constants (K_1 and K_2). Thermodynamic parameters for binding of **2** to D-Man-OMe, 6-*O*-methyl-D-Man-OMe, and D-Man are listed below. Figure S4 shows raw ITC data.

Binding constants and thermodynamic parameters for carbohydrate binding of **2** at 30 °C

Sugar	K_1	ΔH_1	ΔS_1	K_2	ΔH_2	ΔS_2

	(M^{-1})	(cal/mol)	(cal/mol/deg)	(M^{-1})	(cal/mol)	(cal/mol/deg)
D-Man-OMe	1,950	20.0	15.1	123	-393	8.27
6-*O*-Methyl-D-Man-OMe	2,190	21.6	15.4	147	-803	7.26
D-Man	1,680	6.17	14.8	64.3	-162	7.74

Synthesis of PRM-TAMRA (3)

To a solution of **2** (TFA salt, 4.6 mg, 3.99 μmol) in 50 mM MOPS buffer (10.7 mL, pH 7.0) were added TAMRA-alkyne (1.9 mg, 4.06 μmol) in DMSO (400 μL), a premixed solution of 20 mM $CuSO_4$ in distilled water (0.1 mL) and 50 mM THPTA in distilled water (0.2 mL), 100 mM aminoguanidine·HCl in distilled water (1.0 mL), 100 mM sodium ascorbate in distilled water (1.0 mL). The resulting mixture was stirred at room temperature for 23 hr, and then directly adsorbed on a column of Diaion HP-20. After washing with water, the resin was eluted with 70% acetone/water containing 0.1% TFA and the eluate was concentrated *in vacuo*. The residue was purified by reverse-phase HPLC (column: YMC-Pack ODS-A, 5 μm, 20.0 mm ID × 250 mm; solvent: 40-min linear gradient 25% → 60% CH_3CN/water containing 0.1% TFA: flow rate; 8.0 mL/min: UV; 254 nm: Rt; 21.1 min) to afford PRM-TAMRA (**3**) (6.5 mg, 4.00 μmol, quant.) as a TFA salt.

*Characterization data for **3***

$[\alpha]_D$: –248.0 (*c* = 0.05 in MeOH, 25 °C)

HRMS (ESI) : *m/z* = 754.7961 ($[M+H]^{2+}$). Calcd. For $C_{76}H_{87}N_9O_{24}^{2+}$ 754.7929.

^{1}H-NMR (600 MHz, DMSO-d_6) and ^{13}C-NMR (150 MHz, DMSO-d_6) spectra are shown in Figure S5. Signal assignments are shown below.

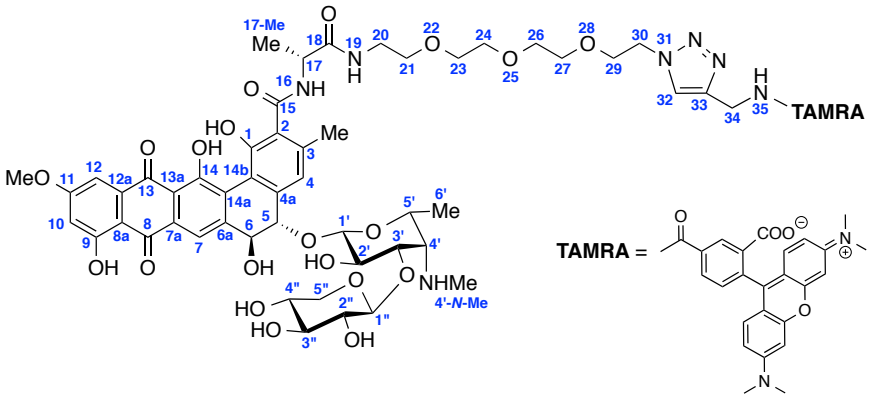

^{1}H-NMR and ^{13}C-NMR signal assignments for PRM-TAMRA (**3**).

Position	^{1}H-NMR (600 Hz)	^{13}C-NMR (125 Hz)
1		151.5
2		127.6
3		136.7
3-Me	2.29 (3H, s)	18.9
4	7.12 (1H, br.s)	ND[a]
4a		137.4
5	4.61 (1H, d, *J* = 8.9 Hz)	80.6
6	4.68 (1H, d, *J* = 8.9 Hz)	71.0
6a		147.3
7	8.02 (1H, br.s)	ND[a]
7a		126.8
8		185.0
8a		110.0
9		164.6
10	6.92 (1H, br.s)	106.6
11		165.9
11-OMe	3.95 (3H, s)	56.3
12	7.28 (1H, d, *J* = 1.7 Hz)	107.4
12a		134.5
13		186.8
13a		115.8
14		157.9
14a		131.2
14b		114.5
15		166.8
16 (NH)	8.27 (1H, d, *J* = 7.2 Hz)	
17	4.47 (1H, m)	48.3
17-Me	1.31 (3H, d, *J* = 7.3 Hz)	17.5
18		172.2
1’	4.77 (1H, d, *J* = 6.8 Hz)	103.7
2’	3.45-3.52 (1H, m)	68.7
3’	3.97 (1H, m)	79.5
4’	3.45-3.52 (1H, m)	63.0
4’-NMe	2.69 (3H, s)	36.1
5’	3.92 (1H, m)	67.3
6’	1.29 (3H, d, *J* = 6.8 Hz)	15.8
1’’	4.48 (1H, d, *J* = 7.4 Hz)	104.9
2’’	3.17 (1H, dd, *J* = 8.5, 7.4 Hz)	73.4
3’’	3.19 (1H, dd, *J* = 8.9, 8.5 Hz)	75.8
4’’	3.34 (1H, m)	69.2
5’’	3.14 (1H, dd, *J* = 11.3, 10.5 Hz), 3.77 (1H, dd, *J* = 11.3, 5.3 Hz)	65.7

19 (NH)	7.85 (1H, br.s)	
20	3.27 (2H, m)	38.6
21, 23, 24, 26, 27	3.45-3.52 (10H, m)	69.4 (3C), 69.5, 69.6
29	3.82 (2H, t, *J* = 5.3 Hz)	68.6
30	4.50 (2H, t, *J* = 5.3 Hz)	49.2
32	7.98 (1H, s)	123.1
33		144.3
34	4.59 (2H, d, *J* = 5.6 Hz)	34.8
35 (NH)	9.32 (1H, t, *J* = 5.6 Hz),	
TAMRA	3.23 (12H, s), 6.88 (2H, br.s), 6.97-7.00 (4H, br.m), 7.54 (1H, d, *J* = 7.8 Hz), 8.31 (1H, d, *J* = 7.8 Hz), 8.69 (1H, s)	40.2 (4C), 96.2 (2C), 112.0 (2C), 113.8 (2C), 128.9, 129.7, 130.1 (2C), 130.9, 131.3, 135.6, 140.2, 156.1 (2C), 156.3 (2C), 157.9, 164.4, 165.8

[a]Not detected due to severe signal broadening.

CuAAC Reaction Analysis of 2 and TAMRA-alkyne

A mixture of 2 mM **2** (2.0 μL) in distilled water, 1 M D-Man-OMe (2.0 μL) in distilled water, and 50 mM MOPS buffer containing 10 mM $CaCl_2$ (8.7 μL, pH 7.0) was pre-incubated at 60 °C for 15 min. To this mixture were added 4 mM TAMRA-alkyne (5 μL) in DMSO, an aliquot (0.3 μL) of a premixed solution of 20 mM $CuSO_4$ in distilled water (0.1 mL) and 50 mM THPTA in distilled water (0.2 mL), 100 mM aminoguanidine·HCl in distilled water (1.0 μL), and 100 mM sodium ascorbate in distilled water (1.0 μL). After incubation at room temperature for 30 min, 5 μL of the reaction mixture was analyzed by HPLC (column: CAPCELL PAK C18 ACR, 5 μm, 4.6 mm ID × 250 mm; solvent: 45-min linear gradient 25% → 60% CH_3CN/water containing 0.1% TFA: flow rate; 1.0 mL/min: UV; 254 nm). Control experiments were similarly conducted in the absence of $CuSO_4$ or D-Man-OMe. HPLC chromatograms of the CuAAC reaction mixtures in the absence (upper) and in the presence of $CuSO_4$ (middle), and in the presence of $CuSO_4$ after pre-incubation with D-Man-OMe (lower) are shown in Figure S6.

Fluorescent Staining Experiment

Candida rugosa AJ 14513 was grown in YM broth at 30 °C for 48 hr (approximately 10^7 cells/mL). *Escherichia coli* AJ 3837 was grown in LB broth at 37 °C for 20 hr (approximately 10^8 cells/mL). Each culture broth (100 μL) was put in a 1.5 mL-Eppendorf tube, and diluted with sterilized saline (200 μL). After centrifugation at 5,000 rpm (2,100 *g*) for 5 min at 4 °C, the supernatant was

removed by decantation. The remaining cells were washed twice with sterilized saline (200 μL), and suspended with 50 mM MOPS buffer (pH 7.0) containing 1 mM $CaCl_2$ (166 μL). To this suspension was added 20 mM **2** in distilled water (1.0 μL). After incubation for 15 min at room temperature, the reagents were added in the following order: 4 mM TAMRA-alkyne in DMSO (10 μL), aliquot (3 μL) of a premixed solution of 20 mM $CuSO_4$ in distilled water (1 mL) and 50 mM THPTA in distilled water (2 mL), 100 mM aminoguanidine·HCl in distilled water (10 μL), 100 mM sodium ascorbate in distilled water (10 μL). The resulting mixture was shaken with a voltex mixer for a few second, and incubated for 1 hr at room temperature in the dark. After centrifugation at 5,000 rpm (2,100 *g*) for 5 min at 4 °C, the supernatant was removed by decantation. The remaining cells were washed three times with 50 mM MOPS buffer (pH 7.0) containing 1 mM $CaCl_2$ (400 μL), and re-suspended with the same buffer (100 μL). One drop of the suspension was placed on a slide glass and observed under a fluorescence microscope FSX100 (Olympus, Tokyo, Japan) with a U-MWIG3 filter set (excitation filter: 530-550, emission filter: >575 nm). In the experiments in the absence of **2** or TAMRA-alkyne, distilled water (1.0 μL) or DMSO (10 μL) was added instead of 20 mM **2** or 4 mM TAMRA-alkyne, respectively. All fluorescence images were adjusted for brightness and contrast in Adobe Photoshop Element 8.0. The images for *E. coli* are shown in Figure S7.

DATA AND SOFTWARE AVAILABILITY

The crystallographic data for the [$\mathbf{1}_2$/Ca^{2+}] complex have been deposited in the CCDC under ID code 1856317.